XLI CILAMCE
XLI Ibero-Latin American Congress on Computational Methods in Engineering
16-19 November, 2020 FOZ DO IGUAÇU PARANÁ - BRAZIL

Influence of frost formation in tube-fin evaporators using a distributed model

Caio Cezar Neves Pimenta[1], André Luiz Seixlack[2]

Dep. of Mechanical Engineering, São Paulo State University/UNESP
CEP 15385-00, Av. Brasil, 56, Ilha Solteira/SP, Brazil
[1]*engmeccaiocezar@gmail.com*
[2]*andre.seixlack@unesp.br*

Abstract: Evaporators are heat exchangers of the refrigeration systems used to transfer heat from the refrigerated environment. Their low operating temperatures favor the frost formation on their surfaces that, depending on its thickness, can reduce the evaporator cooling capacity. This work presents a distributed model for analyzing the influence of formation and frost densification on the performance of tube-fin evaporators. The fundamental equations of mass conservation, momentum, and energy conservation are used to model the refrigerant flow. The energy conservation equation of the evaporator tube wall is also solved. On the airside, the equations of mass conservation, momentum, and conservation of energy are employed to simulate the formation and frost growth on the evaporator surface. The system of equations is integrated numerically and solved iteratively by successive substitutions. The numerical results obtained in this work are compared with experimental data available in the open literature. Considering the range of inlet refrigerant temperature, -25.9 to -20.2 °C, the means absolutes deviations, regarding the cooling capacity and the frost mass are 8,1% e 6,0%, respectively. Among all tests carried out, during the four-hour interval there was an average reduction of 8% in the cooling capacity due to the concentration of frost on the surface of the tubes and fins.

Keywords: Tube-fin evaporator. Frost formation. Household refrigerator. Distributed model. Performance.

1 Introduction

Currently, refrigeration systems are essential both to thermal comfort, ensuring good thermal conditions, and to the conservation of foodstuffs, ensuring the quality of products through conservation at low temperatures. Most current refrigeration systems use the vapor compression refrigeration cycle, consisting of four main devices: compressor, condenser, evaporator, and an expansion device or expansion valve.

Evaporators operating at temperatures close to -10 ° C are subject to an inevitable and undesirable physical phenomenon: the formation of frost on their surfaces. Frost is a porous medium formed by the sublimation of water vapor at pressures lower than the triple point of water. The frost accumulation, depending on its thickness, increases the thermal resistance between the tubes and the airflow, makes it difficult the airflow through the evaporator and, consequently, reduces its cooling capacity. Thus, the temperatures in the refrigerated compartment increase and the compressor stays on for a longer time, which increases the energy consumption of the refrigerator. To reduce the problem, the electrical resistance is periodically activated to defrost the evaporator surface. However, this procedure also contributes to increasing energy consumption of the refrigerator, Knabben [1].

The frost formation on the surface of evaporators has aroused the interest of many researchers due to its influence on the performance of these heat exchangers. Reductions up to 40% were observed in the cooling capacity of tube-fin evaporators due to formation of frost, Silva [2].

Hayashi *et al*. [3] evaluated the frost formation process in flat plates experimentally, to obtain a relationship between the external conditions of the flow and the porous medium. The authors observed the growth of frost using equipment and visualization techniques. They noted that this growth depends on the psychometric condition of the air, the plate surface temperature, and the airflow conditions. The frost growth was divided into three stages: (i) frost crystals growth; (ii) frost layer growth; (iii) complete frost layer growth.

Yang, Lee, and Song [4] developed a mathematical model to evaluate the behavior of a tube-fin evaporator subject to the frost formation on the coils and fins, using the mass diffusion equation on the surface of the frost layer. The heat and mass transfer coefficients on the surface of the tubes and fins were calculated by empirical correlations. The model was validated by comparing the thickness of the frost layer and the heat transfer rate calculated with the respective measured values. These comparisons show good agreement with an average deviation of 2.2%. The authors did not provide information on the procedure used to measure the thickness of the frost and about the refrigerant solution procedure that flows into the evaporator.

Silva, Hermes, and Melo [5] presented a model for analyzing the frost formation in tube-fin evaporators under typical operating conditions of light commercial refrigeration systems. The model was based on the equations of the mass, energy, and momentum balances on the airside. The frost formation in the transient regime on the evaporator surface is predicted. The numerical results were compared with the experimental data of pressure drop on the airside, air flow rate, cooling capacity, and frost mass accumulated. All predictions remained within the experimental uncertainty ranges. The effects of the progressive reduction of the air passage area caused by the frost layer on the overall thermal resistance were also evaluated. It was found that the growth of the frost layer is the main cause of the reduction of the heat transfer rate of the evaporator. The frost layer growth caused an increase in the pressure drop on the airside and reduced the air flow rate through the evaporator.

Wu, Hu, and Chu [6] investigated experimentally the ice formation in tube-fin evaporators with different types of fins. The heat transfer resistance has increased, due to the ice formation. The operating conditions adopted were: (a) air temperature from -2 to 7 °C; (b) 80% of relative humidity; (c) airspeed from 0.3 to 1.1 m/s; (d) evaporator surface temperature -19 to -10 °C. Wu, Hu and Chu [6] concluded that: (a) based on the observations of the frost layer, a higher concentration of frost was found near the edges than in the middles of the fins. For a single column of angled fins, more frost develops on the fin in the first row than in the others fins; (b) the fin region accumulates more frost per area unit than the base region, as the air comes into contact with the fin first and its heat exchange area is larger than that of the tube; (c) higher air velocities resulted in the formation of more frost.

Although several studies on the frost formation on the surface of tube-fin evaporators are found in the literature, few of them report the mathematical modeling of the phenomenon. Furthermore, in the models found, the refrigerant fluid flow along the evaporator is not analyzed and, generally, the evaporator surface temperature is considered constant.

This work presents a distributed model for analyzing the influence of frost formation and densification on the performance of tube-fin evaporators, commonly used in “no-frost” refrigerators (see Fig. 1). In this regard, one software was elaborated to simulate the flow of refrigerant inside the tubes and air outside the evaporator with frost formation. The flow of the refrigerant fluid inside the tubes was analyzed using a model previously developed by Pimenta [7], wherein the frost formation was not considered.

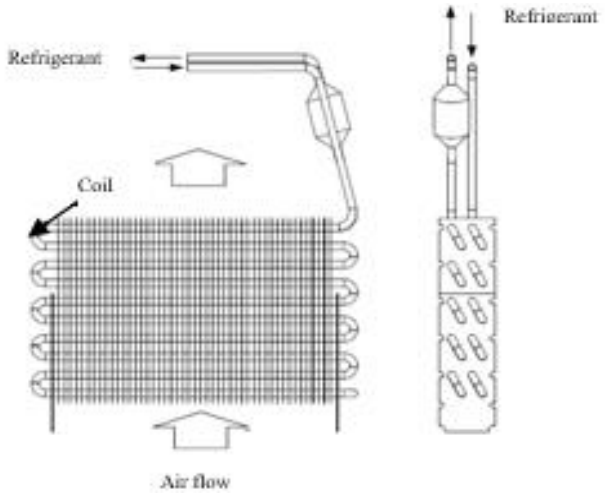

Figure 1 - Tube-fin evaporator used in “no-frost” refrigerators, Knabben [1].

In the Pimenta [7] model the fundamental equations of mass conservation, momentum and energy conservation governing the refrigerant flow are solved in order to evaluate the velocity, pressure and specific enthalpy of the refrigerant fluid, respectively. The energy conservation equation of the evaporator tube wall is also solved to obtain the wall temperature distribution.

This work presents a model implemented on the airside to simulate the formation, growth, and densification of the frost layer on the evaporator surface. The water vapor mass conservation and air energy conservation

equations are solved for calculating of absolute humidity and air temperature, respectively. The pressure drop on the airside is calculated using correlations of the literature. The model is validated by comparing the numerical results obtained with experimental data available in the open literature

The thermo-physical properties of the refrigerant, air and water must be determined and constitutive equations are required to calculate the friction factors, the heat transfer coefficients for the refrigerant and the air and the mass transfer coefficient for the air. Moreover, it is necessary to determine the fins efficiency.

The refrigerant, air and water thermo-physical properties are obtained from REFPROP 8.0 [8]. The thermo-physical properties of the tube wall and fin materials are computed using the data provided by Incropera, Bergman and Lavine [9].

2 Mathematical model

The proposed model consists of the system formed by the equations of mass conservation, momentum and energy conservation for the refrigerant flow, energy conservation at the tube wall, energy conservation and mass conservation of water vapor at airside and mass and energy diffusion equations at the frost layer.

The refrigerant flow inside the tube is divided in two regions: single-phase and two-phase flow. The equations presented below are related to the two-phase flow region. Considering the void fraction $\alpha = 1$, in these equations the governing equations for the superheated vapor region are obtained.

Applying the principle of mass conservation for the refrigerant at the control volume shown in Fig. 2, we obtain

$$\frac{\partial \rho}{\partial t} + \frac{\partial (\rho u)}{\partial z} = 0 \tag{1}$$

where t is the time [s], z is the coordinate along the evaporator tube [m], u is the average velocity of the refrigerant flow in the cross section of the tube [m/s], $\rho = [\alpha \rho_v + (1-\alpha)\rho_l]$ is the density of the liquid-vapor mixture [kg/m^3], $\alpha = \{1 + [\rho_v (1-x)/\rho_l x]\}^{-1}$ is the void fraction and x is the vapor quality. The subscripts l and v indicate the liquid and vapor phases, respectively.

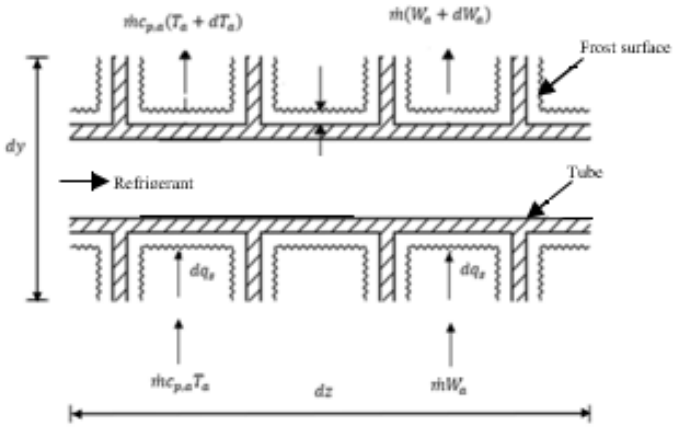

Figure 2 – Control volume for the mass, momentum and energy balance.

Applying the principle of momentum for the refrigerant at the control volume shown in Fig. 2, we obtain

$$\frac{\partial (\rho u)}{\partial t} + \frac{\partial (\rho u^2)}{\partial z} = -\frac{\partial p}{\partial z} - F_z \tag{2}$$

where p is the flow pressure inside the tube [Pa], F_z is the force per volume unit due to friction between the refrigerant and the tube wall [N/m^3]. This term is represented by $F_z = (\partial p/\partial z)_F$, since it represents the portion of the total pressure drop along the volume control, caused by viscous effects. Thus, $F_z = (f \rho u^2 / 2 d_i)$, in which f is the Darcy friction factor and d_i is the inner tube diameter [m].

Applying the principle of energy conservation for the refrigerant at the control volume shown in Fig. 2, we have

$$\frac{\partial \rho i_r}{\partial t} + \frac{\partial}{\partial z}(\rho u i_r) = \frac{\partial p}{\partial t} + \frac{h_{wr} P_i}{A}(T_w - T_r) \tag{3}$$

where $i_r = \left[x i_v + (1-x) i_l\right]$ is the refrigerant specific enthalpy [J/kg], i_l and i_v are the liquid and vapor specific enthalpy [J/kg], respectively, h_{wr} is the convection heat transfer coefficient inside the tube [W/m^{2}K], T_w and T_r are the tube wall and the refrigerant temperatures [°C], respectively, $P_i = (\pi d_i)$ is the inner perimeter of the tube [m] and $A = \left(\pi {d_i}^2/4\right)$ is the cross sectional area of the tube [m^2].

Applying the principle of energy conservation at the tube wall and fins at the control volume shown in Fig. 2, we have

$$m_{wf} c_{wf} \frac{\partial T_w}{\partial t} = \left[U_{aw}(T_a - T_w) + h_m (W_a - W_{a,w}) i_{sv}\right] P_t - h_{wr}(T_w - T_r) P_i \tag{4}$$

where m_{wf} is the mass of the tube wall and fins by unity length [kg/m], $c_{p,wf}$ is the mean specific heat at constant pressure considering the tube and fin materials [J/kg K], U_{aw} is the global heat transfer coefficient between the air and the tube wall [W/m^2 K], T_a is the air temperature [°C], W_a and $W_{a,w}$ are the air absolute humidity and the saturated air humidity at temperature T_w [kg$_v$/kg$_{\text{dry air}}$], respectively, and h_m is the mass transfer coefficient [kg/m^{2}s], determined by the analogy between heat and mass transfer. This coefficient is calculated by the Lewis correlation, [$h_m = h_a / Le\ c_{p,a}$], where Le is the Lewis number, $L_e = [k_a/(\rho_a c_{p,a} D_{ab})]$, D_{ab} is the water-air mass diffusivity [m^2/s], k_a is the air thermal conductivity [W/mK] and $c_{p,a}$ is the specific heat at constant pressure for the air [J/kgK]. $P_t = P_r + P_f \eta_f$ is the total perimeter of heat transfer, P_r is the outer perimeter not covered by fins [m], P_f is the fin surface area per unit length [m] an η_f is the fin efficiency presented by Liang *et al.* [10].

Thus, the model for the refrigerant flow is constituted by the system of Eqs. (1) to (4), which should be solved to give the distributions of u ,p, i_r, and T_w, respectively. To perform this task, closer relationships are then needed to calculate the refrigerant, air and water thermo-physical properties, the friction coefficients, the refrigerant-air heat transfer coefficients and the water mass-transfer coefficient (Pimenta [11]).

Applying the principle of mass conservation and the heat diffusion balance at the frost layer shown in Fig. 2, we have the model equations for the airside (Hermes *et al.* [12])

$$T_{a,i+1} = T_{sg} - (T_{sg} - T_{a,i}) exp\left(-\frac{h_a A_t}{\dot{m}_a c_{p,a}}\right) \tag{5}$$

$$W_{a,i+1} = W_{a,sg} - (W_{a,sg} - W_{a,i}) exp\left(-\frac{h_m A_t}{\dot{m}_a}\right) \tag{6}$$

$$W_{a,sg} = W_{a,w} \cosh\left(\sqrt{\frac{\tau \lambda x_g}{\varepsilon D_{ab}}}\right) \tag{7}$$

$$T_{sg} = T_w + \frac{q^{"} x_g}{k_g} + \frac{i_{sv} \rho_a D_{ab} \varepsilon_g W_{a,w}}{k_g \tau_g}\left[1 - \cosh\left(\sqrt{\frac{\tau \lambda x_g}{\varepsilon_g D_{ab}}}\right)\right] \tag{8}$$

$$\frac{dx_g}{dt} = \frac{m_d^{"}}{\rho_g} \tag{9}$$

$$m = \iint m^{"}\, dA dt \tag{10}$$

where the subscript i+1 indicate the control volume exit, T_{sg} is the frost surface temperature [k], A_t is the total contact area between air and the frost surface [m^2], $W_{a,sg}$, is the air absolute humidity at the frost surface, ε_g is the frost porosity, τ_g is the frost tortuosity, i_{sv} is the desublimation latent heat of the water vapor [J/kg], $q^{"}$ is the conduction heat flux at frost layer [W/m^2], k_g, is the frost thermal conductivity [W/mK], D_{ab} is the diffusivity of water vapor in air [m^2/s], $m_d^{"}$ is the mass flux of densification of the frost [kg/m^{2}s], $m^{"}$ is the overall mass flux of the frost [kg/m^{2}s] and m is the frost mass [kg].

Thus, the model for the frost layer is constituted by the system of Eqs. (5) to (10), which should be solved to give the variables $T_{a,i+1}, W_{a,i+1}, W_{a,sg}, T_{sg}, dx_g/dt$ and m, respectively.

3 Solution methodology

The numerical solution for the system of Eqs. (1) to (4) is obtained by numerical integration. The evaporator is divided in small cells, a total of *m*-1 cells, with same dimensions Δz, as shown in Figs. 3 and 4. The governing equations are integrated over time and space, *z* direction, between the points *j*-1 and *j* along the tube (see Fig. 3), obtaining a system of algebraic equations. Unsteady terms in governing equations are discretized using the approximation formula: $\partial\phi/\partial t = [(\phi - \phi^o)/\Delta t]$, in which the superscript "o" means the time step immediately before. For the integrals over time a completely implicit scheme was used, in order to reach numerical stability for the algorithm.

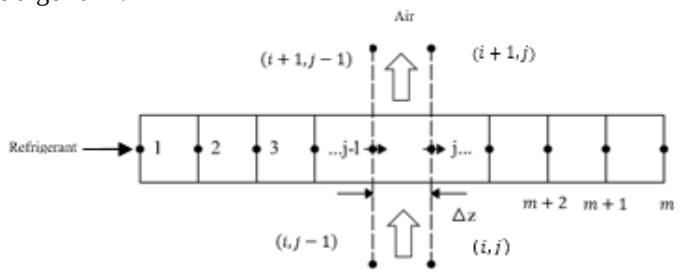

Figura 3 - Discretization of the evaporator tube for the numerical solution.

The discretized equations for calculating the variables present the same form for all points. To avoid the use of a separate equation for the point *j*=1, the evaporator inlet, a dummy cell is used in this position. Variables *u*, *p*, i_r and T_w are stored at the *j*-1 and *j* points of the cell, shown in Fig. 3, while the variables T_a and W_a are stored on the *(i,j), (i,j-1), (i+1,j)* and *(i+1,j-1)* points of the cell, also shown in Fig. 3.

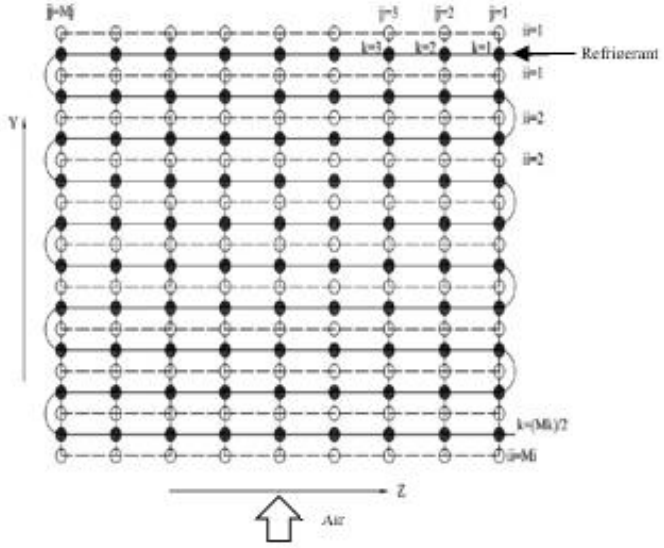

(a)

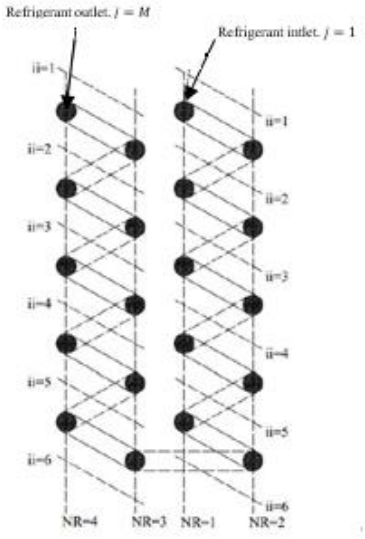

(b)

Figure 4. Discretization of the evaporator for the numerical solution: (a) front view; (b) lateral view.

The solution of the resulting algebraic system of equations is obtained for each cell along the evaporator and the variables *u* ,*p*, i_r, T_w, W_a and T_a are calculated at every point. To improve the efficiency of the solution process, a two-level iterative method is used. First, the refrigerant and tube wall variables are calculated. Second, the air variables are calculated.

The evaporator tubes are arranged in four rows, with five tubes per row, as shown schematically in Figs. 4(a) and 4(b). For the grid shown in Fig. 4(b), *NR* index relates to the line, *ii* refers to the vertical position of the tubes and *jj* refers to a horizontal position along the tubes.

Once the operating conditions and dimensions of the evaporator are known, the model allows calculating the performance of the evaporator, the cooling capacity, the frost mass, the pressure drop and the air flow rate.

For a given evaporator coil configuration, the simulation process starts with a set of air and refrigerant inlet conditions. The mass flow rate, $\dot{m}_r$, the quality, x, and the temperature of the refrigerant, T_r, are provided at the

coil inlet, $z = 0$. The air mass flow, $\dot{m}_a$, relative humidity, ϕ, and air temperature, T_a, are provided at the evaporator inlet.

The solution of the equations is obtained for each point along the evaporator, by the successive substitution method, calculating the variables: u, p, i_r, and T_w, for the refrigerant flow. With the properties of the air and the conditions of the tube, the variables for the airside are calculated: T_a, W_a, $\rho_g, k_g, T_s, x_g, \tau$ and ε, also by the successive substitution method. Convergence is obtained point by point from the each evaporator division, when the variation of the calculated variables reaches a variation less than 10^{-4}.

4 Results and Discussion

This work presents some comparisons between results computed using the present model and experimental data obtained by Knabben [1] in a tube-fin evaporator with two rows and four tubes per row, using the refrigerant R134a. These comparisons are made regarding the cooling capacity, the accumulated frost mass, the pressure drop on the airside and the air flow rate, all evaluated over a period of four hours. Table 1 shows the geometrical parameters for the evaporator analyzed by Knabben [1] and the operating conditions are: refrigerant temperature at the evaporator inlet in the range of -25,9 to -20,2°C, relative humidity in the range of 39,6 to 44,7%, air flow rate of 46 m^3/h and initial frost thickness of 0,001 mm.

Table 1. Geometrical parameters of the evaporator analyzed by Knabben [1].

Geometrical parameters			
Straight tube length (mm)	340	Longitudinal tube spacing (mm)	23
Deep (mm)	60	Tube inner diameter (mm)	6,3
Total coil length (m)	6,8	Tube outer diameter (mm)	8,0
High (mm)	190	Fins thickness (mm)	0,22
Transversal tube spacing (mm)	22	Number of fins per tube	52

Figures 5(a) and 5(b) show the comparisons between measured and calculated cooling capacity and frost mass, respectively. These figures show the results obtained by the present model in its complete form (complete model), and also the results obtained by the present model, but considering the wall temperature constant and equal to the evaporation temperature, T_w=T_{evap}=cte, that is, without solving the refrigerant and tube wall equations (simplified model).

As can be seen in Fig. 5(a), approximately 87% of the cooling capacity calculated by the complete model and by the model with T_w=T_{evap} are within ±10% of the experimental ones. Furthermore, the average absolute deviation was 8.8%, considering all tests performed, which demonstrates the quality of the proposed model. Note in Figure 5 (b), that approximately 60% of the frost mass calculated by the models are within ±15% of the experimental ones and the average absolute deviation was 6.2%, considering all tests performed.

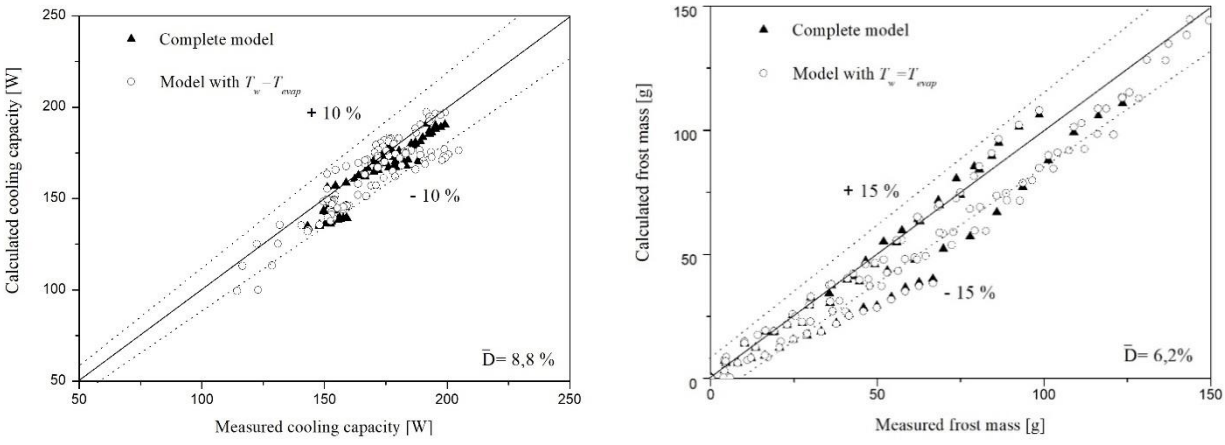

(a) (b)

Figure 4 - Comparison between measured (Knabben [1]) and predicted: (a) cooling capacity; (b) frost mass.

Figures 6(a) and 6(b) show the comparisons between measured and calculated pressure drop and air flow rate, respectively. It can be seen in Fig. 6(a) that, approximately 72% of the pressure drop calculated by the complete model and by the model with T_w=T_{evap} are within ±15% of the experimental ones. Furthermore, the average absolute deviation was 1.5%, considering all tests performed. Figure 6(b) shows that, approximately

90% of the air flow rate calculated by the models are within ±15% of the experimental ones and the average absolute deviation was 1.7%, considering all tests performed.

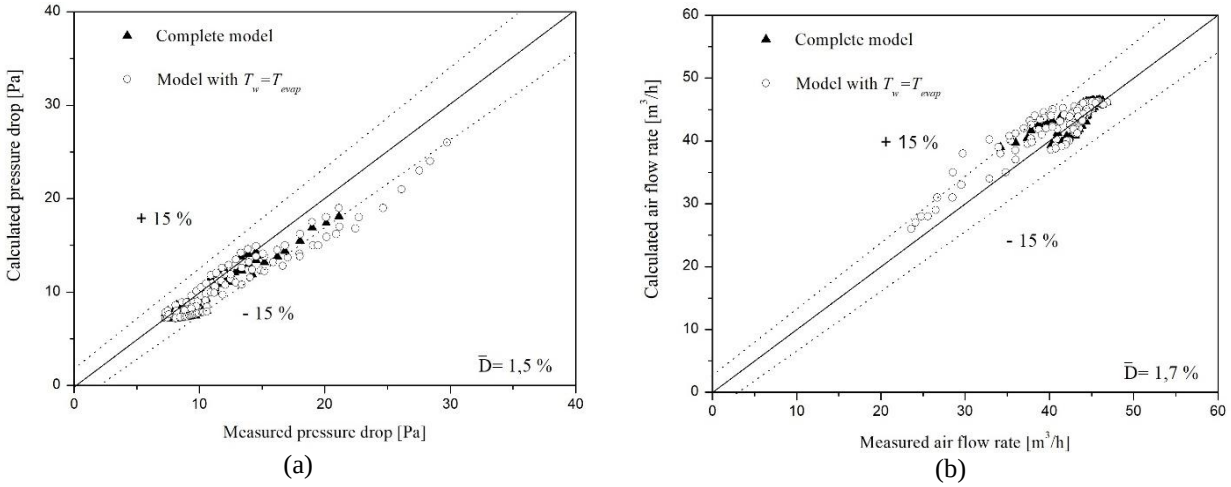

(a) (b)

Figure 6 - Comparison between measured (Knabben [1]) and predicted: (a) pressure drop; (b) air flow rate.

5 Conclusions

This work presents a distributed model for analyzing the influence of formation and frost densification on the performance of tube-fin evaporators, commonly used in "no-frost" refrigerators. The governing equations of the refrigerant flow are integrated over time and space, obtaining a system of algebraic equations that is solved with the frost equations, by successive substitution method. The analysis of the formation and frost densification was based on the model developed by Hermes *et al.* [12].

Comparison between experimental results obtained by Knabben [1] and those obtained in this work show good agreement with regard to the cooling capacity, frost mass, pressure drop, as well as air flow rate. Considering all tests performed, over a period of 4 hours, during which the formation, growth and density of the frost layer was evaluated, the mean absolute deviations between the calculated results and the experimental data were: (i) 8.1% for the cooling capacity; (ii) 6.0% for the frost mass formed; (iii) 1.0% for the pressure drop on the airside; (iv) 1.2% for the air flow rate.

References

[1] F. T. Knabben. An IN-SITU Study of Frost Formation in No-frost Evaporators. Master Thesis. University of Santa Catarina. (in Portuguese). 2010.

[2] D. L. Silva,. Analysis of Ice and Frost Formation and its Effect on the Thermo-hydraulic Performance of Finned Tube Evaporators. PhD Thesis. University of Santa Catarina. (in Portuguese). 2012.

[3] Y. Hayashi, Y., A. Aoki, S. Adashi and K. Hori. "Study of frost properties correlating with frost formation types". *ASME Journal of Heat Transfer*, vol. 99, pp. 239-245, 1977.

[4] D. K. Yang, K. S. Lee and S. Song, Simon. "Modeling for predicting frosting behavior of a fin–tube heat exchanger". *International Journal of Heat and Mass Transfer*, vol. 49, n. 7-8, pp. 1472-1479, 2006.

[5] D. L. Silva, C. J. L. Hermes and C. Melo. "Experimental study of frost accumulation on fan-supplied tube-fin evaporators". *Applied Thermal Engineering*, vol. 31, n. 6, pp. 1013-1020, 2011.

[6] X. Wu, S. Hu and F. Chu. "Experimental study of frost formation on cold surfaces with various fin layouts". *Applied Thermal Engineering*, vol. 95, pp. 95-105, 2016.

[7] P.H.N. Pimenta. Distibuted Model Applied for Analyzing of Tube-fin Evaporators. MSc. Thesis. São Paulo State University, Ilha Solteira, Brazil. (in Portuguese). 2015.

[8] E.W. Lemmon, M. L. Huber and M. O. McLinden, *NIST Reference Fluid Thermodynamic and Transport Properties – REFPROP, Version 8.0*. NIST, Standard Reference Database 23, Gaithersburg, 2007.

[9] F.P Incropera, T. L. Bergman and A.S. Lavine, *Fundamentos de transferência de calor e de massa*. 8ª. ed. Rio de Janeiro: LTC, 648 p., 2019.

[10] S.Y. Liang, M. Liu, T.N. Wong and G.K. Nathan. "Analytical study of evaporator coil in humid environment". *Applied Thermal Engineering*, vol. 19, n. 11, p. 1129-1145, 1999.

[11] C.C.N. Pimenta, Influence of Frost Formation in Tube-Fined Evaporators Using a Distributed Model. MSc. Thesis. São Paulo State University, Ilha Solteira, Brazil. (in Portuguese). 2019.

[12] C.J.L. Hermes, R, O. Piucco, J.R. Barbosa JR. and C. Melo, "A study of frost growth and densification on flat surfaces". *Experimental Thermal and Fluids Sciencie*, vol. 33, pp. 371-379, 2009.